Synthesis of Ordered Porous Graphitic-C3N4 and Regularly Arranged Ta3N5 Nanoparticles by Using Self-Assembled Silica Nanospheres as a Primary Template

ARTICLE *in* CHEMISTRY - AN ASIAN JOURNAL · JANUARY 2011

Impact Factor: 4.59 · DOI: 10.1002/asia.201000523 · Source: PubMed

6 AUTHORS, INCLUDING:

Kazuhiro Takanabe
King Abdullah University of Science and Te…
125 PUBLICATIONS **4,413** CITATIONS
SEE PROFILE

Atsushi Shimojima
Waseda University
104 PUBLICATIONS **2,062** CITATIONS
SEE PROFILE

CHEMISTRY
AN ASIAN JOURNAL

DOI: 10.1002/asia.201000523

Synthesis of Ordered Porous Graphitic-C_3N_4 and Regularly Arranged Ta_3N_5 Nanoparticles by Using Self-Assembled Silica Nanospheres as a Primary Template

Yuki Fukasawa,[a] Kazuhiro Takanabe,[a] Atsushi Shimojima,[a] Markus Antonietti,[b] Kazunari Domen,[a] and Tatsuya Okubo*[a]

Abstract: Uniform-sized silica nanospheres (SNSs) assembled into close-packed structures were used as a primary template for ordered porous graphitic carbon nitride (g-C_3N_4), which was subsequently used as a hard template to generate regularly arranged Ta_3N_5 nanoparticles of well-controlled size. Inverse opal g-C_3N_4 structures with the uniform pore size of 20–80 nm were synthesized by polymerization of cyanamide and subsequent dissolution of the SNSs with an aqueous HF solution. Back-filling of the C_3N_4 pores with tantalum precursors, followed by nitridation in an NH_3 flow gave regularly arranged, crystalline Ta_3N_5 nanoparticles that are connected with each other. The surface areas of the Ta_3N_5 samples were as high as 60 $m^2 g^{-1}$, and their particle size was tunable from 20 to 80 nm, which reflects the pore size of g-C_3N_4. Polycrystalline hollow nanoparticles of Ta_3N_5 were also obtained by infiltration of a reduced amount of the tantalum source into the g-C_3N_4 template. An improved photocatalytic activity for H_2 evolution on the assembly of the Ta_3N_5 nanoparticles under visible-light irradiation was attained as compared with that on a conventional Ta_3N_5 bulk material with low surface area.

Keywords: carbon nitride · nanoparticles · photocatalysis · silica nanospheres · tantalum nitride

Introduction

Nanostructured inorganic materials have attracted increasing attention owing to their wide applications based on their unique properties. Broader research activity has so far been conducted on bottom-up syntheses of nanostructured materials from soluble precursors;[1] however, precise control over the composition, structure, and morphology is still an ongoing subject of research.

One of the successful examples of the formation of oxide nanoparticles with controlled size is our liquid-phase method to generate uniform-sized (< 50 nm) silica nanospheres (hereafter designated as SNSs) in an emulsion system containing tetraethyl orthosilicate (TEOS) and water with basic amino acids.[2] The basic amino acids act as a weak-base catalyst as well as a buffer solution to achieve the slow hydrolysis of TEOS whilst maintaining a constant pH value during the synthesis. Upon solvent evaporation, these SNSs self-assemble into close-packed structures with three-dimensional, interparticle voids with high uniformity. These self-assembled SNSs are promising as a hard template to give nanomaterials with an inverse-opal structure,[2a,c,d] which can be further utilized to produce arrays of metal-oxide nanoparticles.[2e]

Polymer or silica particles and their colloidal crystals have been extensively used as hard templates to produce porous materials.[3,4] The examples include synthesis of porous graphitic C_3N_4 (g-C_3N_4); that is, mesoporosity and macroporosity were successfully imparted into g-C_3N_4 by heating the mixture of cyanamide and different-sized colloidal silica spheres, followed by removal of the silica template.[5,6] Furthermore, porous g-C_3N_4 has also emerged as a new class of

[a] Y. Fukasawa, Dr. K. Takanabe, Dr. A. Shimojima, Prof. K. Domen, Prof. T. Okubo
Department of Chemical System Engineering
The University of Tokyo, 7-3-1 Hongo, Bunkyo-ku
Tokyo 113-8656 (Japan)
Fax: (+81) 3-5800-3806
E-mail: okubo@chemsys.t.u-tokyo.ac.jp

[b] Dr. M. Antonietti
Department of Colloid Chemistry
Max-Planck-Institute of Colloids and Interfaces
Research Campus Golm, 14424 Potsdam (Germany)

Supporting information for this article is available on the WWW under http://dx.doi.org/10.1002/asia.201000523.

hard templates that are useful for producing metal-nitride nanoparticles.[4] A distinct property of the g-C_3N_4 template from the conventional porous carbon template[2c,d,e] is that g-C_3N_4 completely decomposes into nitrogen and cyano fragments at temperatures higher than approximately 950 K, even under an inert atmosphere (e.g., N_2 or Ar),[4] whereas carbon has to be gasified in the presence of oxygen. The cyano fragments derived from g-C_3N_4 serve as a nitrogen source to convert metal precursors into metal nitrides. These characteristics are advantageous for synthesizing various metal nitride nanoparticles such as TiN, VN, and GaN.[4]

Some metal (oxy)nitrides have recently attracted tremendous attention as visible-light-responsive photocatalysts.[7] Among such nitrides, the Ta_3N_5 photocatalyst, with tantalum being in the preferable d^0 electronic configuration, can absorb a large fraction of visible light up to 600 nm, and was reported to produce hydrogen or oxygen in the presence of appropriate sacrificial reagents under visible-light irradiation.[8] This report suggests that the Ta_3N_5 photocatalyst has a suitable band structure for overall water splitting in which a bottom of the conduction band and a top of the conduction band straddle the water redox potentials (required average redox gap: 1.23 eV). Nevertheless, overall water splitting has never been achieved with Ta_3N_5 to date. One promising approach to improve the photocatalytic activity of (oxy)nitride is the synthesis of nano-sized crystals, which are expected to show higher activity than bulk ones because of their larger surface areas and shorter migration distance of photogenerated electrons and holes, thus reducing the chance of their recombination.[9] High crystallinity is also required because the defects present in the low-crystallinity materials are known to enhance the recombination of the photoexcited charges.

Very recently, it was reported that Ta_3N_5 nanoparticles were synthesized by using mesoporous g-C_3N_4 as a decomposable template.[10] The thermal treatment of a tantalum-precursor/mesoporous g-C_3N_4 composite in flowing ammonia was effectively applied to the synthesis of Ta_3N_5 nanoparticles with the d^0 electronic structure. This result is in contrast to the formation of photocatalytically inactive TaN (d^2 electronic structure) nanoparticles in inert gas, such as nitrogen or argon. The obtained Ta_3N_5 nanoparticles showed enhanced photocatalytic activity for hydrogen production under visible-light irradiation.[10] The particle size of Ta_3N_5 was controlled by the pore size of g-C_3N_4 template down to approximately 7 nm, reflecting the particle size of LUDOX silica colloids used as a primary template.[5,6,10] However, ordered arrangements of the Ta_3N_5 nanoparticles have not been attained, though fine control of the nanostructure should be important for both fundamental research and photocatalytic applications.

In this study, we used self-assembled SNSs with a close-packed configuration as a starting template for the synthesis of ordered porous g-C_3N_4, which was then employed as a template for the synthesis of regularly arranged Ta_3N_5 nanoparticles (Scheme 1). By utilizing the voids of the SNSs, the process first produces highly porous g-C_3N_4 with a well-ordered inverse opal structure. The close-packed configuration of the template would eventually lead to Ta_3N_5 nanoparticles with controlled diameters, which may influence the crystallinity whilst ensuring enhanced mass-transfer diffusion in the cavity. The photocatalytic activity of these nanoporous Ta_3N_5 structures for photocatalytic hydrogen evolution was also examined.

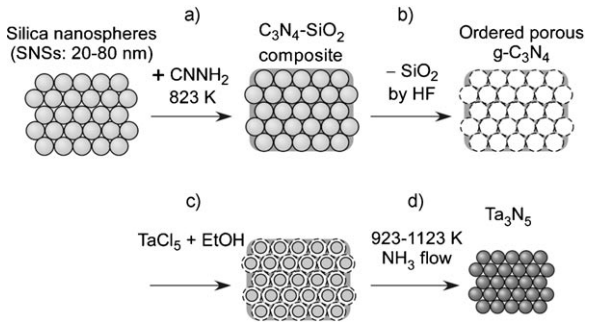

Scheme 1. Schematic illustration of the synthesis of ordered porous g-C_3N_4 and regularly arranged Ta_3N_5 nanoparticles by using close-packed silica nanospheres (SNSs) as the primary template. a) Infiltration of cyanamide followed by polymerization at 823 K, b) removal of silica template by HF treatment, c) infiltration of Ta source followed by drying in air, d) nitridation at 923–1123 K under a flow of NH_3.

Results and Discussion

Synthesis of Ordered Porous g-C_3N_4 by Using SNSs Templates

Figure 1a shows the SEM images of the SNSs after solvent evaporation. The figure clearly shows the spherical SNSs with a uniform-size distribution that are regularly arranged in a close-packed configuration. The diameters of approximately 20, 30, 50, and 80 nm were successfully attained by varying the TEOS amount and the recycling number during the regrowth process of the SNSs. These materials have interparticle narrow voids that are tunable by the sphere size, allowing confined growth of g-C_3N_4 from cyanamide.

Infiltration and polymerization of cyanamide within these interparticle voids of SNSs followed by the removal of silica gave ordered porous g-C_3N_4. The SEM images (Figure 1b) show the inverse opal structure of the g-C_3N_4 products with the spherical pores reflecting the size of the used SNSs. It can be seen from the figure that, for C_3N_4 with relatively large pores (50 and 80 nm), some of the pores are connected to the adjacent ones. The formation of g-C_3N_4 frameworks was confirmed by X-ray diffraction (XRD), FTIR, and CHN elemental analyses. The XRD patterns of the products show a broad peak at $2\theta = 27.3°$ ($d = 0.33$ nm) corresponding to the interlayer distance between g-C_3N_4 sheets (see Figure S1 in the Supporting Information).[6] The FTIR spectra (see Figure S2 in the Supporting Information) show characteristic absorption bands of g-C_3N_4 (1240–1630 cm^{-1} owing to νC=N and νC-N)[5] and no absorption bands associated with the silica template (e.g., at 1000–1200 cm^{-1} owing to

CHEMISTRY
AN ASIAN JOURNAL

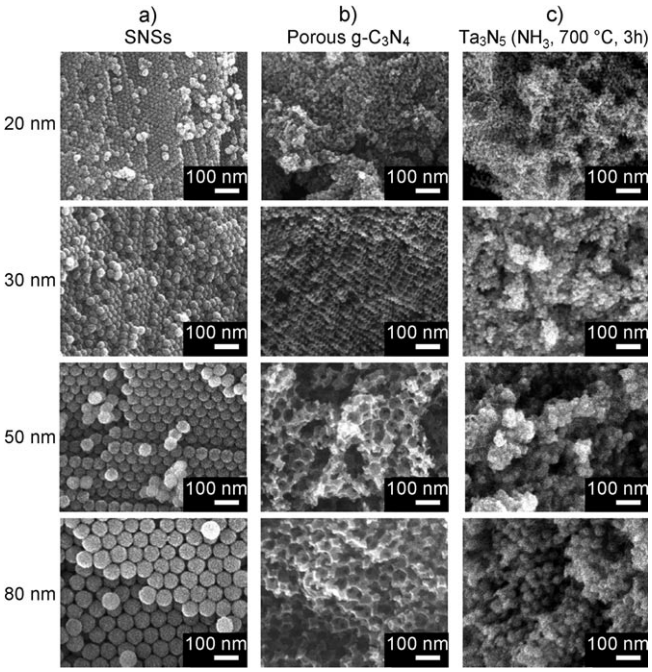

Figure 1. FE-SEM images of a) silica nanospheres (SNSs) after solvent evaporation, b) g-C_3N_4, and c) Ta_3N_5.

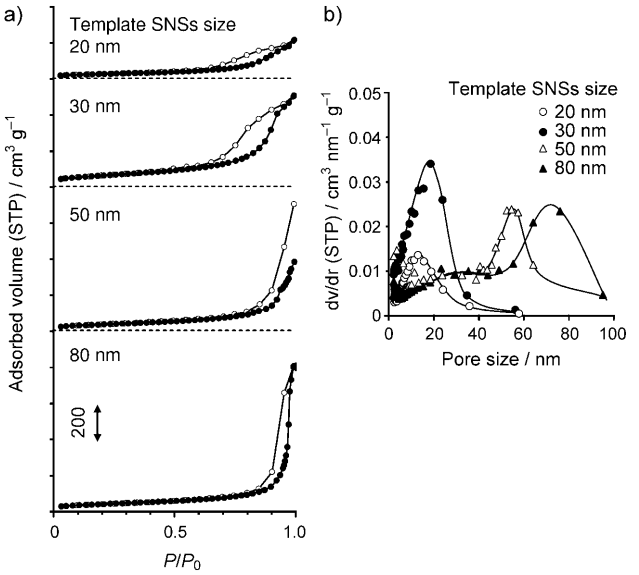

Figure 2. a) Nitrogen adsorption–desorption isotherms, b) BJH pore-size distributions for g-C_3N_4. STP = Standard condition for temperature and pressure; 100 kPa and 273.15 K.

Table 1. Structural parameters of the synthesized g-C_3N_4 and Ta_3N_5.

SNS size[a] [nm]	g-C_3N_4			Ta_3N_5	
	BJH pore size [nm]	BET surface area [m^2g^{-1}]	Pore volume [$cm^{-3}g^{-1}$]	BET surface area [m^2g^{-1}]	Crystallite size[b] [nm]
20	13	98	0.33	60	22
30	20	230	0.79	60	16
50	55	140	1.05	46	20
80	70	140	1.70	36	21
reference	–	–	–	15	30

[a] Diameter of the silica nanospheres used as primary template. [b] Calculated by Scherrer's equation.

νSi-O-Si). The C/N ratios for all of the samples were approximately 0.70, which is smaller than the theoretical value of 0.75. This small ratio is attributed to the existence of residual amino groups, as also previously reported for mesoporous g-C_3N_4 derived from cyanamide.[6] Thermogravimetry analysis showed complete weight loss during heating up to 973 K, confirming the complete removal of the silica template by the HF treatment.

The porous structure of the g-C_3N_4 products was characterized by nitrogen adsorption–desorption measurements. The isotherms and the Barrett–Joyner–Halenda (BJH) pore size distributions are shown in Figure 2, and the Brunauer–Emmett–Teller (BET) surface areas, BJH pore sizes, and pore volumes are compiled in Table 1. The average pore diameter and pore volume of the g-C_3N_4 samples monotonically increased with increasing the size of the SNSs. The average pore sizes were 13, 20, 55, and 70 nm when the diameters of SNSs were 20, 30, 50, and 80 nm, respectively. The pore volume increased from 0.33 cm^3g^{-1} to 1.70 cm^3g^{-1}, with increasing the SNSs diameter from 20 to 80 nm. Assuming that all of the g-C_3N_4 products have spherical pores, the surface area should be inversely proportional to the pore size. However, the surface area becomes the highest for the sample prepared with 30 nm SNSs (~230 m^2g^{-1}), even compared with the one prepared with 20 nm SNSs (98 m^2g^{-1}). It is likely that very narrow interparticle voids in the close-packed arrangement of the SNSs with small diameters (<30 nm) would lead to the formation of less-stable g-C_3N_4 frameworks because of the small wall thickness and the lateral size of each g-C_3N_4 sheet. The low surface area of the sample prepared with 20 nm SNSs is probably owing to partial collapse of the g-C_3N_4 frameworks upon removal of the silica template. This speculation is consistent with the fact that only nonporous, bulk g-C_3N_4 was obtained when SNS 15 nm in diameter was used as a template. This result is in contrast to the previous results on the successful synthesis of g-C_3N_4 with high surface area (up to 440 m^2g^{-1}) by polymerization of cyanamide in the presence of homogeneously dispersed colloidal silica nanoparticles (LUDOX silica).[6] In this case, it appears that thicker and more-extended g-C_3N_4 frameworks can be formed because silica nanoparticles are not tightly interconnected. Such a difference in the g-C_3N_4 frameworks affected the pore size after the template removal. It is also noted that the pore sizes of g-C_3N_4 are apparently smaller than the diameters of the original SNSs. This is possibly because of the shrinkage of g-C_3N_4 frameworks upon the template removal, which was also reported in the case of macroporous g-C_3N_4 prepared by using close-packed, submicron-sized colloidal silica template,[5] but not

in the case of mesoporous g-C_3N_4 templated with LUDOX silica.[6]

A certain amount of vaporized intermediates might be condensed on the outside of the silica template to produce nonporous g-C_3N_4. The presence of such non-porous parts should result in the decrease of the specific surface area of C_3N_4. It appears, however, that non-porous g-C_3N_4 would not affect the subsequent Ta_3N_5 synthesis step as long as the right pores are generated because they cannot act as a template but simply decomposed during heating as described in the following section.

Synthesis of Ta_3N_5 Nanoparticles

The treatment of porous g-C_3N_4 impregnated with tantalum precursors under NH_3 flow at high temperatures (>900 K) caused both nitridation of the tantalum species and decomposition of the g-C_3N_4 template, leading to the formation of nano-particulate Ta_3N_5. The XRD patterns of Ta_3N_5 prepared at 973 K by using the g-C_3N_4 templates with various pore sizes are shown in Figure 3. All of the samples exhibit similar patterns consisting of the peaks ascribed to Ta_3N_5 without any impurity phase. During heat treatment, C_3N_4 likely decomposes to form volatile melamine and cyanic fragments. The elimination of the g-C_3N_4 template was confirmed by elemental analysis showing the low carbon content (<0.1 wt%) in these samples. No clear indication of C–N species in both C1s and N1s regions of XPS analysis (not shown) supports this result. The crystal sizes calculated by Scherrer's equation are around 20 nm, which is independent of the pore size of the g-C_3N_4 template (Table 1). The smaller size of the Ta_3N_5 crystals compared with the pore size of g-C_3N_4 implies that crystal growth occurred before the destruction of the g-C_3N_4 frameworks. It further suggests that the nitridation process was significantly influenced by the NH_3 gases rather than nitrogen present in C_3N_4, which generally form a reduced form of tantalum (Ta^{3+}, i.e., TaN rather than Ta^{5+}; see Figure S3 in the Supporting Information). The NH_3 treatment was thus essential for generating Ta_3N_5 that has d^0 electronic configuration required for water-splitting function.

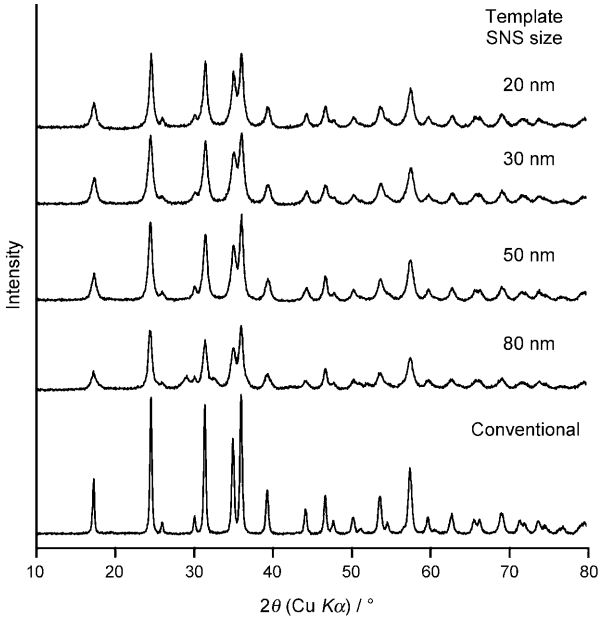

Figure 3. Powder XRD patterns of Ta_3N_5 prepared at 973 K by using ordered porous g-C_3N_4 as a template along with that of conventional Ta_3N_5 particles.

The SEM images of Ta_3N_5 show that aggregates of uniform-sized nanoparticles are orderly arranged (Figure 1c), which is as expected from the observed pore windows present in the porous g-C_3N_4 templates (Figure 1b). The average size of the Ta_3N_5 particles becomes larger with increasing the pore size of the g-C_3N_4 template, clearly indicating that the ordered porous g-C_3N_4 served as the templates to produce Ta_3N_5 nanoparticles. Their particle shape and arrangement well reflected the original silica template (Figure 1a). Interestingly, the TEM image of Ta_3N_5 prepared by using 80 nm SNSs as a primary template (Figure 4a) shows hollow

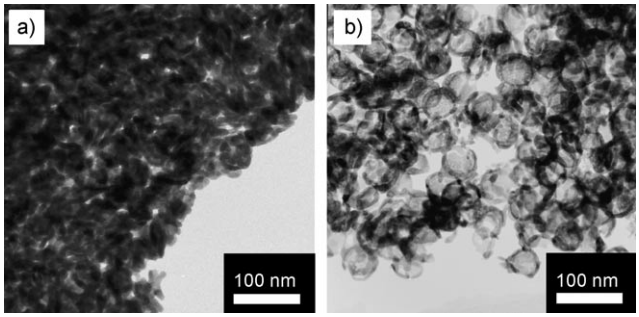

Figure 4. Typical TEM images of Ta_3N_5 prepared with SNSs with a diameter of 80 nm, treated in a NH_3 flow at 973 K. The Ta precursors were impregnated in porous g-C_3N_4 with a) three impregnation cycles, and b) one impregnation cycle, in step (c) in Scheme 1.

structure comprised of several crystallites. This is indicative of incomplete filling of the pores with the tantalum source. When the tantalum amount was further reduced by decreasing the infiltration cycle of tantalum species from three times to once, well-defined hollow spheres with smaller shell thickness were obtained (Figure 4b), although the arrangement of the particles became less ordered.

Nitrogen adsorption–desorption measurements revealed relatively high surface areas of up to 60 $m^2 g^{-1}$ for Ta_3N_5 prepared by using 30-nm SNSs as a primary template (Table 1). The BET surface area of Ta_3N_5 decreased with increasing the size of original SNS templates from 30 to 80 nm, consistent with the formation of the larger nanoparticles. The relatively low surface area of Ta_3N_5 prepared by using 20-nm SNSs should be caused by the less-ordered pore structure of the g-C_3N_4 template, as discussed above. These surface areas were indeed comparable with those prepared with a LUDOX colloidal silica with a diameter of 7 nm (61 $m^2 g^{-1}$).[10]

The UV/VIS diffuse reflectance spectra of the Ta_3N_5 samples are shown in Figure 5a. All of the samples absorb light

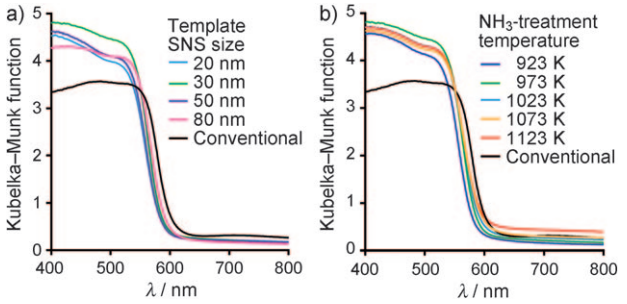

Figure 5. UV/VIS diffuse reflectance spectra of a) Ta_3N_5 treated in NH_3 flow at 973 K and b) Ta_3N_5 prepared with SNSs with a diameter of 30 nm, treated in NH_3 flow at various temperatures. The spectra for conventional Ta_3N_5 particles (see the Supporting Information, Figure S5) are also shown for comparison.

at wavelengths shorter than 600 nm.[8] Compared with the conventional Ta_3N_5 particles, the absorption edges for the prepared Ta_3N_5 samples were slightly shifted to a shorter wavelength, suggesting that these materials have slightly wider band gaps. Considering the crystal size generated in this process (>20 nm), it is unlikely that this shift was owing to the quantum size effects, and no clear correlation was observed between the particle size and the absorption edges. These shifts were also observed for the Ta_3N_5 nanoparticles prepared with mesoporous g-C_3N_4 templated with the LUDOX colloidal silica.[10] It is notable that the absorption beyond 600 nm, assignable to absorption by the defects and the reduced tantalum species, was reduced compared with the conventional Ta_3N_5 sample.

These results demonstrate that the use of the ordered porous g-C_3N_4 template provides an efficient approach to porous Ta_3N_5 consisting of regularly arranged nanoparticles with controlled diameters. By using the porous g-C_3N_4 prepared with the original SNS template of 30-nm diameter, Ta_3N_5 samples were synthesized at various NH_3 treatment temperatures ranging from 923 to 1123 K. The XRD measurements confirmed the formation of Ta_3N_5 single phase at all temperatures (see Figure S4 in the Supporting Information). Even at 923 K, the Ta_3N_5 phase started to form after 1 h of nitridation (data not shown) and obtained as a single phase after 3 h. Crystallization of the Ta_3N_5 phase at such low temperatures in a short time is advantageous for preventing excessive growth and/or aggregation of the particles. The BET surface areas of Ta_3N_5 prepared at 923, 973, 1023, 1073, and 1123 K for 3 h were 57, 60, 46, 40, and 36 m^2g^{-1}, respectively, exhibiting a decrease with an increase in the NH_3 treatment temperature, as expected. UV/VIS spectra for the samples prepared at different NH_3 treatment temperatures are shown in Figure 5b. It appears that the NH_3 treatment at lower nitridation temperatures caused a slight blue shift of the absorption edges (λ = 550–600 nm). Additionally, the spectra for the Ta_3N_5 nanoparticles were nitridated at higher temperatures show higher baselines at wavelengths longer than 600 nm (Figure 5b), which is indicative of the presence of more defects in the Ta_3N_5 structure.

We also examined a two-step heating process including air treatment followed by NH_3 treatment, instead of direct NH_3 treatment. The XRD patterns of the samples are shown in Figure 6. The air treatment of the tantalum species–C_3N_4 composite at 973 K for 3 h led to crystalline Ta_2O_5 nanoparticles, reflecting the size of the original SNS particles. This suggests that the porous g-C_3N_4 can serve as effective templates to give confinements to determine the size of oxide nanoparticles. When these oxide nanoparticles were treated at 973 K under NH_3 atmosphere, a much longer time (~13 h) was required to obtain Ta_3N_5 as a single phase (Figure 6). The resulting Ta_3N_5 still possessed a high BET surface area (43 m^2g^{-1}), although the value is smaller than that achieved by the direct NH_3 treatment (60 m^2g^{-1}). It is expected that this oxidation–nitridation process will enable us to synthesize oxynitride nanoparticles, such as TaON, which is also known as a photocatalyst.[11]

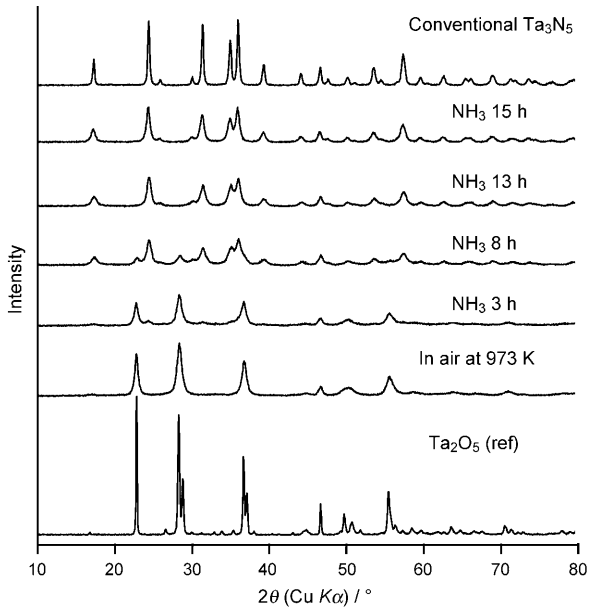

Figure 6. Powder XRD patterns of Ta_3N_5 prepared by a two-step heating process first in air, followed by NH_3 for different duration times (3–15 h) at 973 K by using an ordered porous g-C_3N_4 as the template along with that of conventional Ta_3N_5 particles.

Photocatalytic Reactions Using Ta_3N_5 Nanoparticles

It is known that Ta_3N_5 can work as a photocatalyst possessing suitable band positions for water splitting under visible light irradiation.[8] It was reported that splitting of water into hydrogen or oxygen occurred on Ta_3N_5 in the presence of sacrificial reagents.[8] In this study, we examined photocatalytic hydrogen evolutions from methanol aqueous solution on the prepared Ta_3N_5 samples. Figure 7 shows time courses of evolved H_2 for the Ta_3N_5 photocatalysts prepared at 973 K in NH_3 with the SNS in different sizes (Figure 7a) and the Ta_3N_5 photocatalysts prepared in NH_3 at different

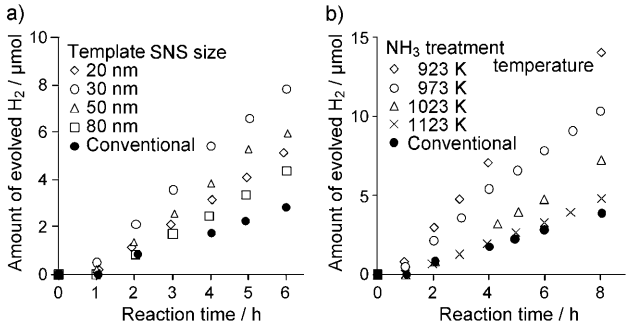

Figure 7. Photocatalytic hydrogen evolution by using the synthesized Ta_3N_5 dispersed in an aqueous solution containing a sacrificial reagent under visible light irradiation (0.1 g cat.; 3 wt% Pt; 300 W Xe lamp; 10 vol% methanol aqueous solution, 100 mL; Pyrex upper-irradiation vessel).

temperatures with the 30-nm SNSs (Figure 7b). For all of the samples prepared from porous g-C_3N_4 templates with different pore sizes (Figure 7a), rates of hydrogen evolution were 1.6 to 4 times higher than that of conventional submicron particles. In general, the higher the surface area was (Table 1), the higher the photocatalytic activity was (Figure 7a). These results are consistent with our recent results that the photocatalytic activity of the high-surface-area-Ta_3N_5 nanoparticles (61 $m^2 g^{-1}$), synthesized by using mesoporous g-C_3N_4 as templates, was one order of magnitude greater than the conventional Ta_3N_5.[10] In addition, at lower nitridation temperature, the photocatalytic activity for H_2 evolution was higher (Figure 7b). As discussed previously, the extent of the absorption beyond the band gap of the materials (~600 nm) in the UV/VIS spectra was lower when the samples were synthesized at lower nitridation temperature. This is indicative of the lower extent of the number of defect sites in the photocatalysts. The improved photocatalytic activity was thus attributable to the decrease in the defects that may act as charge-recombination sites.

High surface area of the photocatalysts can lead to more surface reaction sites, thus possibly enhancing the photocatalytic activity (by enhancing the rates of charge separation and surface redox reactions) when surface reactions are kinetically relevant. The smaller particle size of the photocatalysts may result in a shorter diffusion length for photoexcited electron-hole pairs, thus reducing the chance of recombination as long as the crystallinity in the bulk is kept high, although the surface is generally considered as defects. It should also be noted that the UV/VIS spectra (Figure 5) show the lower extent of absorption beyond 600 nm that is correlated with the presence of reduced tantalum sites and defects. These defect sites are considered to work as charge recombination centers, and therefore the removal of such sites is preferred to improve photocatalytic activity. The improved photocatalytic activity of the Ta_3N_5 nanoparticles developed in this study can be attributed to the high crystallinity with enhanced surface area owing to small particle size.

If the small size with high surface area of the nanoparticles and the fewer number of the defect sites are the exclusive reason for the observed improvement of the photocatalytic activity, other photocatalytic reactions should also be enhanced by using these photocatalysts. The rates for photocatalytic evolution of oxygen from 0.01 M $AgNO_3$ aqueous solution were, however, much lower than that of the conventional submicron-sized Ta_3N_5 particles (data not shown). One explanation would be the different dopant levels that cause the negative shift in the Fermi level of the photocatalyst, relative to water redox potentials. If the bands are shifted to negative without altering the band gap, it is generally accepted that H_2 evolution is enhanced while O_2 evolution is suppressed, especially when the band gap of the photocatalyst is becoming small. At the moment, the differences in photocatalytic activity for these Ta_3N_5 photocatalysts remain unclear, however, our method provides a strategy to have high surface area materials with high crystallinity to aid further development of the photocatalysts.

Conclusions

Ordered *meso*- or macroporous g-C_3N_4 samples were prepared by polymerization of cyanamide by using close-packed SNSs as a primary template. Then, regularly arranged Ta_3N_5 nanoparticles were synthesized by using the porous g-C_3N_4 as a template. Ta_3N_5 nanoparticles with high surface areas were obtained by heating tantalum alkoxide precursors within the porous g-C_3N_4 template under ammonia atmosphere. The particle size was controllable from approximately 15 nm to 50 nm by varying the size of the SNSs in the range of 20 nm to 80 nm. A periodical arrangement of crystalline Ta_3N_5 nanoparticles was confirmed by an electron-microscopic observation. The rates of photocatalytic H_2 evolution under visible-light irradiation by using the Ta_3N_5 nanoparticles were greatly enhanced over the conventional Ta_3N_5 macroparticles.

Experimental Section

Synthesis of silica nanospheres (SNSs): Close-packed silica nanospheres were prepared based on the procedure reported previously.[2] Tetraethyl orthosilicate (TEOS; 10.88 g, 0.05 mol; >96% purity, Tokyo Chemical Industry Co. LTD) was added to the solution of L-lysine (0.146 g, 1 mmol; >97% purity, Tokyo Chemical Industry Co. LTD) in distilled water (138.6 g, 7.7 mol), and the biphasic mixture was stirred at 333 K for 1 day to give a clear dispersion of SNSs with a diameter of approximately 15 nm. Regrowth of the SNSs was achieved by adding TEOS to the seed dispersion, followed by stirring at 353 K for 1 day. The diameter of the SNSs was carefully adjusted to 20, 30, 50, and 80 nm by varying the amount of TEOS and the number of regrowth cycles. After the regrowth processes, the dispersions of the SNSs were evaporated to dryness in an oven at 333 K. During evaporation, SNSs were self-assembled into a close-packed configuration. Finally, the obtained solids were treated in static air at 823 K for 5 h to remove L-lysine.

Synthesis of porous g-C_3N_4: Porous g-C_3N_4 with an inverse-opal structure was synthesized by polymerization of cyanamide within the voids of close-packed SNSs (20–80 nm).[6] The powders of SNSs (10 g) and cyanamide (4.5 g; Aldrich, 99% purity) were heated to 343 K for 30 min to allow filling of the interparticle voids of SNSs with molten cyanamide. The mixture of SNSs and cyanamide was cooled to room temperature

while mixing. After grinding, the SiO_2/cyanamide composite was put in a crucible with a lid and heated to 823 K for 4 h in air without flow to form g-C_3N_4. To remove the silica template, the SiO_2/g-C_3N_4 composite was soaked in 250 g of 10 wt% HF aqueous solution for 1 day without stirring and the resulting solids were then recovered by filtration and washed with water and ethanol. This HF treatment was performed twice to ensure complete removal of the silica. Pale-yellow powders of g-C_3N_4 were finally obtained by drying in an oven at 333 K.

Synthesis of Ta_3N_5 nanoparticles: $TaCl_5$ (8 g; 99.9% purity, Kojundo Chemicals) was added to ethanol (8 g; 99.5% purity, Wako Chemicals) and stirred at room temperature for 5 min under nitrogen atmosphere to give mostly $Ta(OC_2H_5)_5$. The synthesized porous g-C_3N_4 (3.0 g) was added to this solution and stirred for 40 min, and was then recovered by filtration, washed with a small amount of ethanol, and dried in an oven at 333 K overnight to complete hydrolysis and polycondensation of $Ta(OC_2H_5)_5$. For the g-C_3N_4 samples prepared with 50 and 80 nm SNSs, this infiltration cycle of tantalum precursor was repeated twice and three times, respectively. The resulting tantalum species-C_3N_4 composite was heated at varying temperatures in the range of 823 to 1123 K for 3 h in a tubular alumina furnace (ID: 26 mmϕ) under NH_3 flow (50 mL min^{-1}). Crystallization of Ta_3N_5 and decomposition of g-C_3N_4 occurred over 823 K and Ta_3N_5 was obtained as vermilion red powders. For comparison, submicron Ta_3N_5 particles were synthesized as we reported previously.[8] Briefly, Ta_2O_5 (99.9%, Kojundo Chemical) was nitrided under NH_3 flow (500 mL min^{-1}) at 1123 K for 15 h. The SEM image of this sample is shown in Figure S5.

Photocatalytic reaction: Before the reactions, 3 wt% of Pt was loaded on Ta_3N_5 by impregnation by using an aqueous solution of H_2PtCl_6 (Wako Chemicals). The sample was then treated in flowing H_2 at 473 K for 1 h in a separate reactor. The catalyst (0.1 g) was then transferred to a Pyrex top-irradiation-type vessel connected to a closed gas-recirculation system and suspended in an aqueous solution with methanol (10 vol%, 100 mL). The reactant solution was initially evacuated to completely remove the air and irradiated by using a 300W Xe lamp (INOTEX) through a cut-off filter (HOYA L-42; $\lambda > 420$ nm). The reactant solution was maintained at 298 K by a flow of cooling water during the reaction. The evolved gases were analyzed by a gas chromatograph equipped with a thermal conductivity detector (Shimadzu GC-8 A, molecular sieve 5 Å column, Ar as a carrier gas).

Characterization: Nitrogen adsorption–desorption isotherms at 77 K were measured by using Autosorb-1-MP (Quantachrome Instrument Co). The samples were dried under vacuum before the measurements. Powder X-ray diffraction (XRD) patterns were obtained with M03X-HF (Bruker AXS) by using $Cu_{K\alpha}$ radiation. CHN elemental analyses were performed on CE-440 (Elemental Analysis, Inc.). Transmission electron microscopic (TEM) observations were performed with a JEOL JEM 2010 electron microscope at an accelerating voltage of 200 kV. Field-emission scanning electron microscopic (FE-SEM) observations were carried out by using Hitachi S-900 at an accelerating voltage of 6 kV. UV/VIS diffuse reflectance spectra were obtained by using a JASCO V-670 spectrometer equipped with Labsphere diffuse reflectance accessories. X-ray photoelectron spectroscopy (XPS) was conducted by using a JEOL JPS-90SX. Thermogravimetry was performed with a PU 4 K analyzer (Rigaku) in flowing 10% O_2 in He.

Acknowledgements

We thank Dr. Tsuyoshi Takata and Dr. Tsutomu Minegishi for their helpful discussions. This work was supported by the Research and Development in a New Interdisciplinary Field Based on Nanotechnology and Materials Science programs of the Ministry of Education, Culture, Sports, Science and Technology (MEXT) of Japan. This study was also supported by the Global COE program for Chemistry Innovation through Cooperation of Science and Engineering from MEXT of Japan to The University of Tokyo. This work was partly conducted in Center for Nano Lithography & Analysis, The University of Tokyo, supported by MEXT, Japan.

[1] a) A. Henglein, *Chem. Rev.* **1989**, *89*, 1861–1873; b) A. P. Alivisatos, *Science* **1996**, *271*, 933–937; c) T. Trindade, P. O'Brien, N. L. Pickett, *Chem. Mater.* **2001**, *13*, 3843–3858; d) C. Burda, X. B. Chen, R. Narayanan, M. A. El-Sayed, *Chem. Rev.* **2005**, *105*, 1025–1102; e) B. L. Cushing, V. L. Kolesnichenko, C. J. O'Connor, *Chem. Rev.* **2004**, *104*, 3893–3946.

[2] a) T. Yokoi, Y. Sakamoto, O. Terasaki, Y. Kubota, T. Okubo, T. Tatsumi, *J. Am. Chem. Soc.* **2006**, *128*, 13664–13665; b) T. Yokoi, J. Wakabayashi, Y. Otsuka, W. Fan, M. Iwama, R. Watanabe, K. Aramaki, A. Shimojima, T. Tatsumi, T. Okubo, *Chem. Mater.* **2009**, *21*, 3719–3729; c) W. Fan, M. A. Snyder, S. Kumar, P.-S. Lee, W. C. Yoo, A. V. Mccormic, R. L. Penn, A. Stein, M. Tsapatsis, *Nat. Mater.* **2008**, *7*, 984–991; d) T. Yokoi, S. Ohta, R. Watanabe, J. N. Kondo, T. Tatsumi, *Abstracts of the 6th International Mesostructured Materials Symposium (IMMS)*, Belgium, **2008**, Abstract No. P-058; e) J. Sakuma, S. Ohta, H. Imai, T. Yokoi, T. Tatsumi, J. N. Kondo, *Extended abstracts of the 12th Japan-Korea Symposium on Catalysis*, Japan, **2009**, Abstract No. YP15.

[3] a) E. Rossinyol, J. Arbiol, F. Peiro, A. Cornet, J. R. Morante, B. Tian, T. Bo, D. Zhao, *Sens. Actuators B* **2005**, *109*, 57–63; b) H. F. Yang, D. Y. Zhao, *J. Mater. Chem.* **2005**, *15*, 1217–1231; c) A.-H. Lu, F. Schüth, *Adv. Mater.* **2006**, *18*, 1793–1805; d) T. Valdés-Solis, A. B. Fuertes, *Mater. Res. Bull.* **2006**, *41*, 2187–2197; e) M. Kang, S. H. Yi, H. I. Lee, J. E. Yie, J. M. Kim, *Chem. Commun.* **2002**, 1944–1945; f) A.-H. Lu, W. Schmidt, A. Taguchi, B. Spliethoff, B. Tesche, F. Schüth, *Angew. Chem.* **2002**, *114*, 3639–3642; *Angew. Chem. Int. Ed.* **2002**, *41*, 3489–3492; g) H.-J. Liu, W.-J. Cui, L.-H. Jin, C.-X. Wang, Y.-Y. Xia, *J. Mater. Chem.* **2009**, *19*, 3661–3667.

[4] a) A. Fischer, M. Antonietti, A. Thomas, *Adv. Mater.* **2007**, *19*, 264–267; b) A. Thomas, A. Fischer, F. Goettmann, M. Antonietti, J.-O. Müller, R. Schlögl, J. M. Carlsson, *J. Mater. Chem.* **2008**, *18*, 4893–4908.

[5] S. Hwang, S. Lee, J.-S. Yu, *Appl. Surf. Sci.* **2007**, *253*, 5656–5659.

[6] F. Goettmann, A. Fischer, M. Antonietti, A. Thomas, *Angew. Chem.* **2006**, *118*, 4579–4583; *Angew. Chem. Int. Ed.* **2006**, *45*, 4467–4471.

[7] K. Maeda, K. Domen, *J. Phys. Chem. C* **2007**, *111*, 7851–7861.

[8] a) G. Hitoki, A. Ishikawa, T. Takata, J. N. Kondo, M. Hara, K. Domen, *Chem. Lett.* **2002**, *7*, 736–737; b) T. Takata, G. Hitoki, J. N. Kondo, M. Hara, H. Kobayashi, K. Domen, *Res. Chem. Intermed.* **2007**, *33*, 13–25.

[9] J. Zhu, M. Zäch, *Curr. Opin. Colloid Interface Sci.* **2009**, *14*, 260–269.

[10] L. Yuliati, J.-H. Yang, X. Wang, K. Maeda, T. Takata, M. Antonietti, K. Domen, *J. Mater. Chem.* **2010**, *20*, 4295–4298.

[11] G. Hitoki, T. Takata, J. N. Kondo, M. Hara, H. Kobayashi, K. Domen, *Chem. Commun.* **2002**, 1698–1699.

Received: July 28, 2010
Published online: November 24, 2010

